

Hematopoietic Tumors in a Mouse Model of X-linked Chronic Granulomatous Disease after Lentiviral Vector-Mediated Gene Therapy

Raisa Jofra Hernández,^{1,2} Andrea Calabria,^{1,10} Francesca Sanvito,^{2,3,10} Fabiola De Mattia,^{1,10} Giada Farinelli,¹ Serena Scala,¹ Ilaria Visigalli,² Nicola Carriglio,² Maura De Simone,² Michela Vezzoli,² Francesca Cecere,² Maddalena Migliavacca,^{1,4} Luca Basso-Ricci,¹ Maryam Omrani,¹ Fabrizio Benedicenti,¹ Rossana Norata,² Paola Maria Vittoria Rancoita,⁵ Clelia Di Serio,⁵ Paola Albertini,² Patrizia Cristofori,^{2,6} Luigi Naldini,^{1,7} Bernhard Gentner,^{1,8} Eugenio Montini,¹ Alessandro Aiuti,^{1,4,7,9} and Alessandra Mortellaro^{1,9}

¹San Raffaele Telethon Institute for Gene Therapy, IRCCS San Raffaele Scientific Institute, Milan, Italy; ²GLP Test Facility, San Raffaele Telethon Institute for Gene Therapy, IRCCS San Raffaele Scientific Institute, Milan, Italy; ³Pathology Unit, Department of Experimental Oncology, IRCCS San Raffaele Scientific Institute, Milan, Italy; ⁴Pediatric Immunohematology and Bone Marrow Transplantation Unit, IRCCS San Raffaele Scientific Institute, Milan, Italy; ⁵University Centre for Statistics in the Biomedical Sciences, Vita-Salute San Raffaele University, Milan, Italy; ⁶Non-Clinical Safety *In Vivo* Translation Research, Glaxo Smith Kline, Ware, UK; ⁷Medical School, Vita-Salute San Raffaele University, Milan, Italy; ⁸Hematology and Bone Marrow Transplantation Unit, IRCCS San Raffaele Scientific Institute, Milan, Italy

Chronic granulomatous disease (CGD) is a rare inherited disorder due to loss-of-function mutations in genes encoding the NADPH oxidase subunits. Hematopoietic stem and progenitor cell (HSPC) gene therapy (GT) using regulated lentiviral vectors (LVs) has emerged as a promising therapeutic option for CGD patients. We performed non-clinical Good Laboratory Practice (GLP) and laboratory-grade studies to assess the safety and genotoxicity of LV targeting myeloid-specific Gp91^{phox} expression in X-linked chronic granulomatous disease (XCGD) mice. We found persistence of gene-corrected cells for up to 1 year, restoration of Gp91^{phox} expression and NADPH oxidase activity in XCGD phagocytes, and reduced tissue inflammation after LV-mediated HSPC GT. Although most of the mice showed no hematological or biochemical toxicity, a small subset of XCGD GT mice developed T cell lymphoblastic lymphoma (2.94%) and myeloid leukemia (5.88%). No hematological malignancies were identified in C57BL/6 mice transplanted with transduced XCGD HSPCs. Integration pattern analysis revealed an oligoclonal composition with rare dominant clones harboring vector insertions near oncogenes in mice with tumors. Collectively, our data support the long-term efficacy of LV-mediated HSPC GT in XCGD mice and provide a safety warning because the chronic inflammatory XCGD background may contribute to oncogenesis.

INTRODUCTION

Chronic granulomatous disease (CGD) is a rare inherited disorder caused by loss-of-function mutations in the genes encoding the components of the nicotinamide adenine dinucleotide phosphate (NADPH) oxidase responsible for generating free radicals (i.e., reactive oxygen species [ROS] and other intermediates) in neutrophils, monocytes, and macrophages.¹ Because the NADPH oxidase com-

plex is required for the killing of bacterial and fungal microorganisms, affected patients present high susceptibility to recurrent life-threatening infections and suffer from a chronic inflammatory response that together lead to granuloma formation in various organs and premature death.² The majority of CGD cases (~70%) are X-linked inherited due to mutations in the gene encoding the Gp91^{phox} subunit (XCGD), which primarily affect males, while the remaining cases carry autosomal recessive traits affecting both males and females.

Conventional treatments of CGD consist of lifelong prophylactic administration of antibacterial and antifungal agents, interferon gamma (IFN γ), and granulocyte infusions to help prevent and treat infections. However, infections and chronic inflammation still cause significant morbidity and mortality.³ Hematopoietic stem cell (HSC) transplantation (HSCT) from matched or haploidentical donors provides a long-term cure for patients with CGD.^{4–6} Reduced-intensity conditioning regimens may diminish acute morbidity associated with HSCT, potentially relevant in patients with ongoing/recurrent infections. Yet, allogeneic HSCT in CGD requires a careful balancing act between toxicity, infections, graft failure, and graft-versus-host disease (GVHD), which impact the overall and event-free survival.

Gene therapy (GT) using autologous hematopoietic stem and progenitor cells (HSPCs) corrected with a functional gene copy represents

Received 10 April 2020; accepted 20 September 2020;
<https://doi.org/10.1016/j.ymthe.2020.09.030>.

⁹Senior author

¹⁰These authors contributed equally to this work.

Correspondence: Alessandro Aiuti, San Raffaele Telethon Institute for Gene Therapy, IRCCS San Raffaele Scientific Institute, Via Olgettina 60, 20132 Milan, Italy.

E-mail: aiuti.alessandro@hsr.it

an attractive therapeutic option for CGD patients who cannot be considered for conventional HSCT. Clinical trials of GT using autologous HSPCs demonstrated the long-term correction of disease defects in pediatric patients with primary immunodeficiencies (PIDs), including adenosine deaminase (ADA) deficiency,⁷⁻⁹ Wiskott-Aldrich syndrome,¹⁰⁻¹² and X-linked severe combined immunodeficiency (SCID-X1).¹³

The initial GT clinical trials for CGD using autologous CD34⁺ HSPCs transduced *ex vivo* with a γ -retroviral (γ -RV) vector in the absence of bone marrow (BM) conditioning showed the feasibility of the procedure.^{14,15} However, after the initial engraftment of transduced cells, the proportion of gene-corrected granulocytes declined within 3-4 months in most patients,¹⁴ indicating that only a few HSPCs engrafted and suggesting the need for preparative conditioning prior to gene-modified cell infusion. Subsequent phase I GT clinical trials have been conducted in XCGD patients receiving myeloablative conditioning followed by infusion of patients CD34⁺ transduced with a γ -RV vector in which the Gp91^{phox} expression is driven by the Friend mink cell spleen focus-forming virus (SFV) long terminal repeat (LTR).¹⁶⁻²¹ Although gene-marked cells remained detectable in the peripheral blood, only a small proportion of circulating neutrophils showed a functionally reconstituted NADPH oxidase, indicating either a lack of transduction of long-term HSCs or counter selection of transduced cells or a progressive silencing of transgene expression. Nevertheless, the few functionally corrected neutrophils were sufficient to fully or partially resolve pre-existing life-threatening infections. In the German/Swiss study, 4 of the 12 XCGD patients receiving gene-corrected CD34⁺ HSPCs and presenting long-term engraftment developed severe myelodysplasia after therapy because of the expansion of dominant clones carrying the γ -RV integrated within or nearby the proto-oncogenes MDS1-EV11 and PRDM16.^{16,19,21} One patient died of multiorgan failure caused by septic shock, and the others were rescued by allogeneic HSCT.

These studies provide evidence of the potential clinical efficacy of GT for CGD but also highlight the need for a much more effective and safer way to deliver genes into HSPCs. Compared with γ -RV vector, self-inactivating lentiviral vectors (LVs) offer the advantage of short and more efficient transduction of HSPCs accompanied by a reduced risk for insertional mutagenesis, as demonstrated by several mouse and human studies.^{22,23} Different LVs encoding human Gp91^{phox} under the control of a myeloid-specific promoter (MSP) have been developed, and their efficacy was tested in preclinical models.²⁴⁻²⁷ Transduction of mouse BM-derived XCGD lineage-negative (Lin⁻) cells and human XCGD CD34⁺ HSPCs with an LV encoding Gp91^{phox} under a synthetic chimeric myeloid promoter (pCCLchimGp91_s) drove higher Gp91^{phox} expression and NADPH activity in myelomonocytic cells (i.e., neutrophils) and myeloid cell progenitors compared with lymphoid cells *in vitro* and *in vivo*.²⁴ Therapeutic efficacy and no evidence of toxicity were reported in a preclinical study performed according to Good Laboratory Practice (GLP) using a clinical-grade G1XCGD LV to transduce human CD34⁺ XCGD cells and mouse XCGD Lin⁻ cells.²⁵

Initial results from a multicentric phase I/II lentiviral GT trial using the G1XCGD LV have been recently reported.²⁸ Nine patients with severe XCGD received autologous G1XCGD-transduced CD34⁺ following myeloablative conditioning, and safety and efficacy were assessed for a minimum of 12 and a maximum of 36 months. Two patients died within 3 months of treatment for pre-existing comorbidities. VCN and NADPH oxidase activity in blood neutrophils were stable in six of seven patients over 24 months. Analysis of vector integration site (IS) distributions revealed a polyclonal repertoire of gene-modified cells, and none of the most abundant clones did harbor ISs in or nearby MECOM (MDS/EV11). Surviving patients did not experience new bacterial and fungal infections.

Our group developed the dual-targeted MSP.Gp91_126T(2) LV (MSP.Gp91.2T), which allows efficient Gp91^{phox} expression in phagocytic cells (neutrophils and monocytes) and de-targeting in the HSPC compartment.^{26,27} The MSP.Gp91.2T has a self-inactivating configuration, with LTR sequences at the terminal ends, the splice donor and the acceptor site, the ψ encapsidation signal including the 5' portion of the gag gene, a Rev-responsive element, and a woodchuck hepatitis virus post-transcriptional regulatory element. A codon-optimized Gp91^{phox} sequence was cloned downstream a MSP based on a minimal Gp91^{phox} promoter from the endogenous locus fused to the synthetic SP146 element. Two tandem sequences complementary to microRNA-126-3p, which is highly expressed in HSPCs, but not in differentiated cells, were cloned to the 3' of Gp91^{phox} coding sequence, thereby reducing off-target transgene expression. The inclusion of the miR-126 microRNA targets leaves unaltered the potential transactivation activity of the synthetic promoter.

We showed that the MSP.Gp91.2T vector promotes sustained Gp91^{phox} expression and NADPH oxidative activity in human and mouse XCGD myeloid cells, whereas it remained transcriptionally inactive in CD34⁺ cells.²⁶ GT mediated by MSP.Gp91.2T-transduced HSPCs was effective in protecting XCGD mice from *S. aureus* pulmonary infection.²⁷

Despite the extensive investigation of the efficacy of HSPC GT for XCGD in cells and mouse model systems, there is little information about long-term (>5 months) safety and efficacy in non-clinical studies with LV-mediated GT for XCGD.^{24,25} Also, insertional genotoxicity has been conducted by transplanting LV-transduced Lin⁻ cells isolated from CD45.2 C57BL/6 mice into CD45.1 recipients followed up to 26 weeks.²⁷ Although these are undoubtedly useful investigations, they did not take into account the CGD inflammatory background, which might contribute to the emergence of unfavorable events. Therefore, in view of clinical application, we conducted a GLP toxicology and tumorigenicity study in XCGD mice to evaluate the long-term efficacy and potential adverse reactions following LV-mediated HSPC GT. We show the long-term correction of NADPH oxidase activity in peripheral blood granulocytes of XCGD mice receiving GT for up to 1 year in the absence of evident signs of organ toxicity. However, a small subset of XCGD mice receiving transduced XCGD HSPCs showed an oligoclonal insertion profile and developed T cell lymphoma or myeloid leukemia. In contrast, healthy C57BL/6

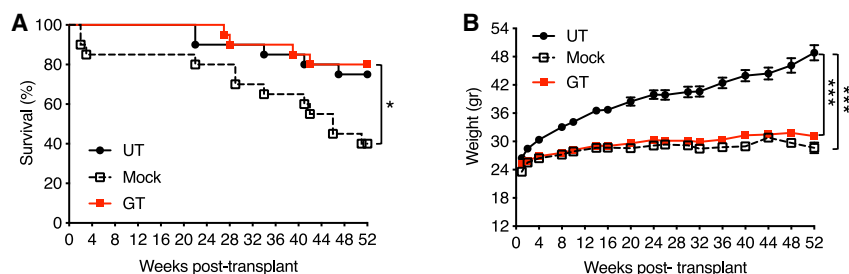


Figure 1. HSPC Gene Therapy Improved the Long-Term Survival of XCGD Mice

(A) Curves compare the survival rate of XCGD UT (n = 20), Mock (n = 20), and GT (n = 20) mice over 52 weeks (*p < 0.05). (B) Body weight changes of mice were monitored weekly in mice of the XCGD Mock and GT groups. Values are given as mean \pm SD. The comparisons among groups were performed only at 52 weeks (***p < 0.001).

mice transplanted with HSPCs isolated from XCGD mice and transduced with the MSP.Gp91.2T LV exhibited a highly polyclonal pattern of LV integrations with no evidence of general toxicity or development of tumors. These findings suggest that the selection pressure as a result of the chronic exposure to the inflammatory milieu, a hallmark of CGD, may have favored the emergence of adverse events from genotoxic insertions.

RESULTS

Evaluation of Systemic Toxicity in XCGD Mice Transplanted with MSP.Gp91.2T-Transduced HSPCs

In view of the prospective clinical development of HSPC GT for XCGD, we executed a GLP toxicology study to assess the long-term term efficacy, toxicity, and tumorigenicity of MSP.Gp91.2T-mediated GT in XCGD mice (Table S1). Lin⁻ HSPCs isolated at high purity (>99%, containing 2.6% of Sca1⁺c-kit⁺ cells) from the BM of donor male Cybb^{-/-} (XCGD) mice were transduced with a purified preparation of the MSP.Gp91.2T LV²⁶ at high-titer virus transduction (multiplicity of infection [MOI] = 200) to ascertain potential toxic effects on transduced cells. Transduced Lin⁻ HSPCs were transplanted into lethally irradiated XCGD male mice (XCGD GT group, n = 20) (Figure S1A). A group of XCGD mice received mock-transduced Lin⁻ HSPCs (XCGD Mock group, n = 20), and a group of non-irradiated age-matched untreated (UT) XCGD mice was included as a control (XCGD UT mice, n = 20). Upon transduction, sca1⁺c-kit⁺ cells were 1.21% and 0.90% in the XCGD Mock and GT groups, respectively (Figure S1B), with a transduction efficiency of 100% and a median vector copy number (VCN) per genome of 2.19 (range 1.03–5.94) in colony-forming units (CFUs) (Figure S1C).

Transplantation of transduced cells was well tolerated by recipient mice. No difference in survival between XCGD GT and UT mice was observed, whereas a substantial proportion (~60%) of XCGD Mock mice died early, possibly because of the combined effect of conditioning and lack of Gp91^{phox} (Figure 1A). Three mice belonging to the XCGD Mock group died shortly after treatment as a result of radiation-related complications and were excluded from the study. On average, XCGD GT and Mock surviving mice gained little weight during the 52 weeks of observation, in contrast with UT mice, because of pre-transplant irradiation (Figure 1B).

Fur discoloration manifested in XCGD GT and Mock groups, but not in XCGD UT mice starting from week 8 related to pre-transplant irra-

diation. Lesions of the skin and eyes, hair loss, and swollen hindlimb, forelimb, and muzzle recurrently occurred in all mice, mostly in XCGD UT mice (UT, 4/20, 20%; Mock, 1/17, 6%; GT, 2/20, 10%), and thus were not related to the transplanted MSP.Gp91.2T-transduced HSPCs.

Clinical chemistry parameters (glucose, total protein) in the blood were similar between XCGD GT and Mock mice at 52 weeks post-transplant, while the levels of alanine aminotransferase (ALT) and aspartate aminotransferase (AST) were lower than in XCGD Mock mice, but within the normal range (Figure S2A), excluding potential toxic effects in kidney, liver, pancreas, gut, and the cardio-circulatory system.

Efficient Long-Term Immune Reconstitution in XCGD Mice after HSPC GT

We evaluated the degree of hematopoietic and immune reconstitution achieved post-GT in XCGD recipient mice by hemogram and flow cytometry analyses in the peripheral blood at 11, 30, and 50 weeks after transplantation. Hematological analysis showed that erythrocyte and hemoglobin (HGB) levels were comparable between XCGD Mock and GT at 50 weeks post-transplant, but lower compared with wild-type (WT) and XCGD UT, probably because of myeloablative conditioning (Figure S2B). Circulating platelet (PLT) number was similar in all groups. XCGD Mock and UT mice showed elevated total white blood cells (WBCs), which returned to normal in XCGD GT mice, with amelioration of the inflammatory background (Figure S2B).

The proportion of T cells in peripheral blood of XCGD GT mice was similar to that of WT mice at 11 and 30 weeks and increased in XCGD GT mice at 52 weeks post-treatment (Figure S3A). B cells and monocytes were comparable between XCGD Mock and GT mice at all time points (Figure S3A). Peripheral blood granulocytes were higher in XCGD GT mice compared with XCGD Mock mice at 30 and 50 weeks post-transplant (Figure S3A). No differences were observed in the lymphoid and myeloid compartments of the spleen and BM of XCGD Mock and GT mice at 52 weeks post-transplant (Figures S3B and S3C). Long-term multi-lineage HSCs (multipotential progenitor [MPP]), myeloid (granulocyte-macrophage progenitor [GMP]), lymphoid (granulocyte-macrophage-lymphocyte progenitor [GMLP]), and erythroid (MEP, ERY) progenitors were detected in the BM of XCGD GT and Mock mice at similar levels

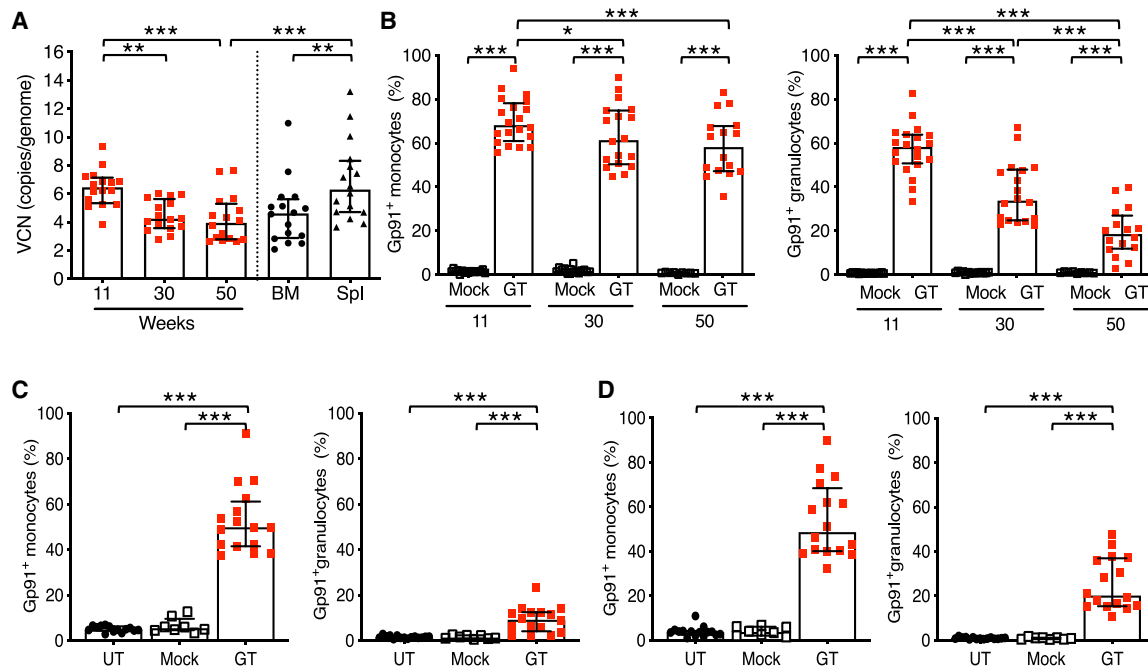


Figure 2. Gene Therapy Specifically Restored Gp91^{phox} Expression in Myeloid Cells of Peripheral Blood, BM, and Spleen of XCGD GT Mice

(A) Determination of VCN in peripheral blood leukocytes at 11, 30, and 50 weeks after treatment, and BM cells and splenocytes of XCGD GT mice at termination (52 weeks), as assessed by quantitative PCR (qPCR) using a Viia7 Real-Time PCR System. Values are given as median and interquartile range. * $p < 0.05$; ** $p < 0.01$; *** $p < 0.001$. (B–D) Gp91^{phox} expression was measured in monocytes and Ly6G⁺ granulocytes isolated from peripheral blood at the indicated time points (B), spleen (C), and BM (52 weeks) (D) of XCGD UT, Mock, and GT mice. Values are given as median and interquartile range. For data shown in (B), post hoc comparisons were performed within a group among time points and within a time point among groups. *** $p < 0.001$.

(Figures S3D and S3E). The observed similarities in the primary immune cell subsets in XCGD GT mice and age-matched UT and WT mice are indicative of a successful recovery of the size of these peripheral immune cell pools after GT.

The MSP.Gp91.2T LV Effectively Restored Gp91^{phox} Expression and NADPH Oxidative Activity in XCGD GT Mice

We determined whether MSP.Gp91.2T-mediated HSPC transduction can lead to the correction of the genetic defect in XCGD GT mice. Vector-positive cells were detected in peripheral blood leukocytes with a median VCN value per genome of 6.45, 4.24, and 3.95 at 11, 30, and 50 weeks post-treatment (Figure 2A). A higher median VCN value was detected in splenocytes compared with total BM cells (6.29 versus 4.62, respectively) at 52 weeks post-treatment (Figure 2A).

We then measured the surface expression of human Gp91^{phox} in XCGD GT mice. Gp91^{phox} was expressed by ~68% and ~60% of peripheral blood monocytes and granulocytes, respectively, of XCGD GT mice at 11 weeks post-GT, whereas the Gp91^{phox} expression remained very low or undetectable in T and B cells (Figure 2B; Figure S4). Although the proportion of Gp91^{phox}-positive monocytes remained stable (median ~60%) in the peripheral blood at 30 and 50 weeks, the fraction of Gp91^{phox}-expressing granulocytes declined from the median value of 60% to ~20% at 50 weeks after GT (Figure 2B). The percentage of Gp91^{phox}-positive monocytes was higher

than that of gene-corrected granulocytes in the spleen and BM (Figures 2C and 2D).

Next, we assessed the activity of NADPH oxidase in myeloid cells isolated from XCGD GT mice receiving transduced HSPCs by a standard dihydrorhodamine (DHR) assay.²⁹ NADPH oxidase activity was fully corrected in peripheral blood granulocytes of XCGD GT mice and reached ~40% of normal levels in monocytes (Figure 3A). A similar trend was present in the granulocytes and monocytes of the BM compared with peripheral blood (Figure 3B). A noteworthy decreased incidence and degree of severity of acidophilic macrophagic pneumonia with the disappearance of abscesses and neutrophilic inflammatory cell infiltrate were observed in the lungs of XCGD GT mice, indicating that the reconstituted NADPH oxidase activity corrected the pulmonary CGD phenotype (Figure 3C).

Collectively, these data indicate that the MSP.Gp91.2T LV vector restores long-term physiological NADPH-mediated superoxide production, which effectively eradicates the respiratory tract infections typically present in the XCGD mouse model.

Evaluation of the Long-Term Toxicity and Tumorigenicity following MSP.Gp91-Mediated Transduction in Mouse HSPCs

Mortality was observed in mice of each experimental group throughout the study, starting from week 22. We performed full

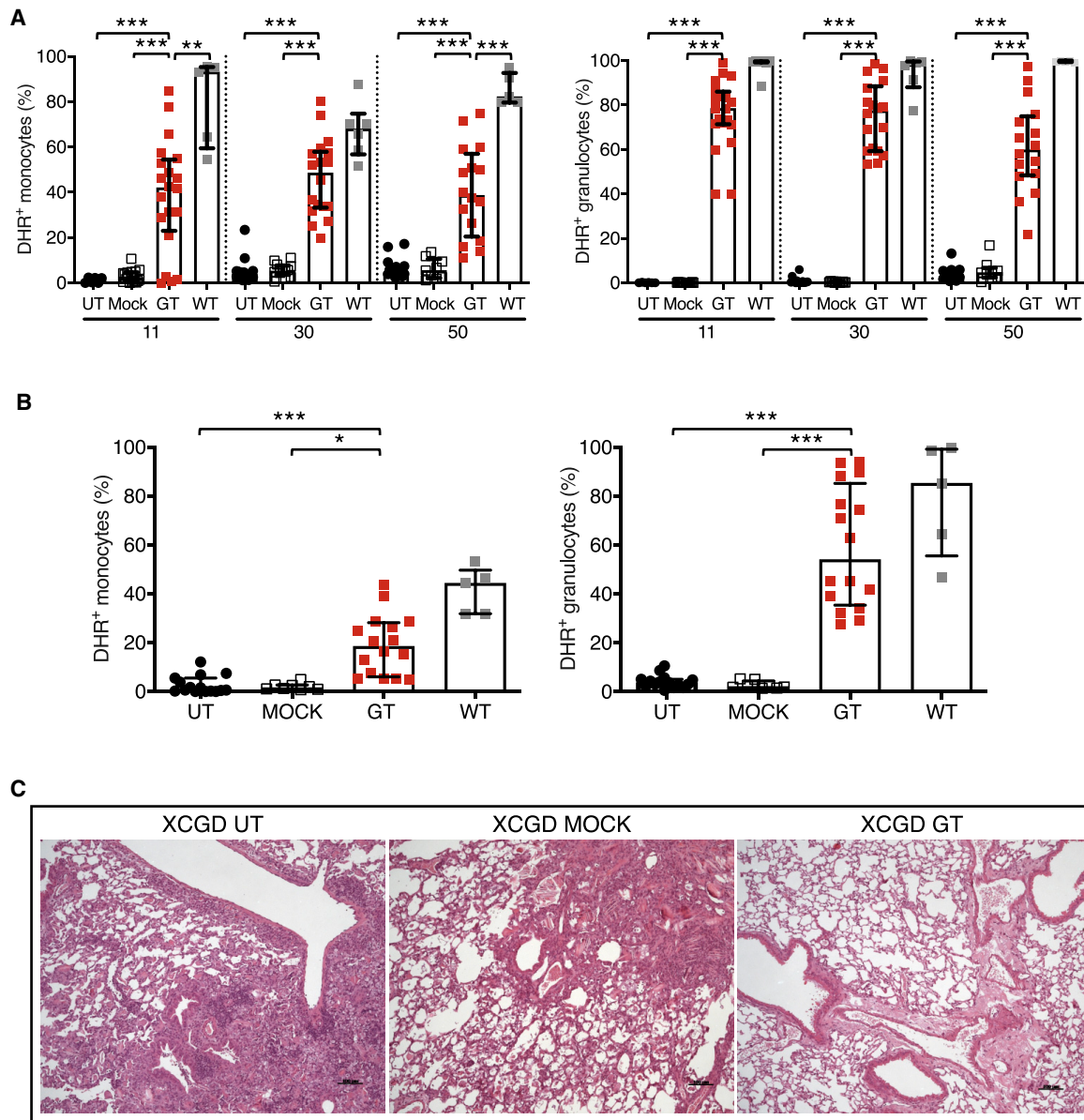


Figure 3. Restoration of NADPH Oxidase Activity in Mononuclear Phagocytes of XCGD GT Mice Corrects Pulmonary Inflammation

(A and B) NADPH oxidase activity was measured in monocytes and granulocytes of the peripheral blood (A) and BM (B) of XCGD UT, Mock, and GT mice by a dihydro-rhodamine (DHR) assay for flow cytometric detection. The reference values for age-matched wild-type (WT) mice were also shown. Statistical difference was shown for comparisons between XCGD GT mice versus the other groups (** $p < 0.01$; *** $p < 0.001$). (C) Hematoxylin and eosin (H&E) staining of sections of lungs of XCGD UT, Mock, and GT mice. Original magnification 100 \times ; scale bars: 100 μm . * $p < 0.05$.

necropsy and histopathological evaluation of tissues of interim unscheduled deaths and terminal killed. The spleen of XCGD UT mice was characterized by marked expansion of the red pulp with increased extramedullary hematopoiesis and the high presence of myeloperoxidase (MPO)-positive myeloid cells (Figure 4A). We also noticed increased cellularity of F4/80⁺ histiocytes/macrophages in the BM of XCGD UT mice, which correlated to elevated levels of inflammatory cytokines, including interleukin

(IL)-1 β , CCL5, and IL-12p40, in the BM milieu (Figures 4B and 4C).

The most likely causes of premature death are summarized in Table S2. Morbidity related to the CGD phenotype was observed in 4 out of 5 XCGD UT mice and in 3 out of 9 XCGD Mock mice euthanized because of poor health conditions. These mice showed swollen hindlimb/forelimb, enlarged muzzle, enlarged mandibular lymph nodes,

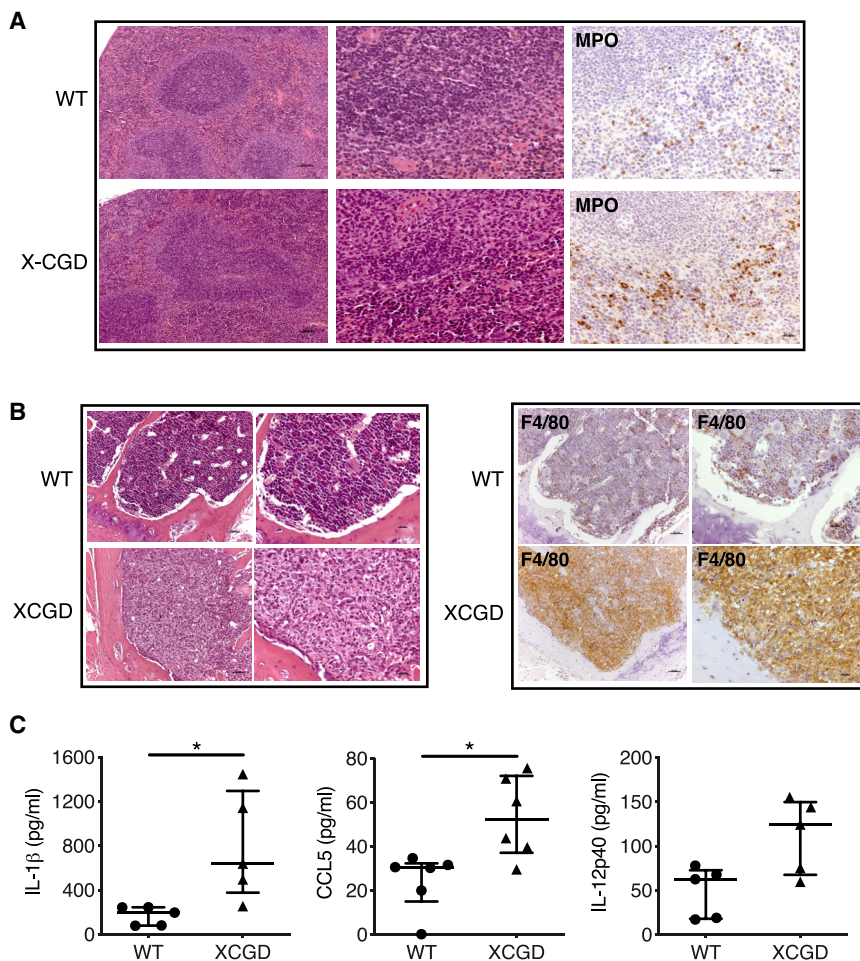


Figure 4. Tissue and Systemic Inflammation in XCGD Mice

(A and B) H&E sections of the spleen (A) and BM (B) of WT and XCGD mice. Consecutive sections were stained with H&E or immune stained with myeloperoxidase (MPO) and F4/80 antibodies. Spleen: original magnification 100 \times ; scale bars, 100 μ m; original magnification 200 \times , scale bars, 20 μ m. BM: original magnification 200 \times , scale bars, 50 μ m; original magnification 400 \times , scale bars, 20 μ m. (C) Cytokines in the milieu of total BM collected from XCGD and WT mice measured by multiplex bead assay. Values are given as mean \pm SEM. * $p < 0.05$.

GT mice with similar incidence and degree of severity. Proliferative lesions, such as bronchioalveolar and gastrointestinal adenomas, adenocarcinomas, cortical adenomas, and benign medullary tumor of adrenal glands, observed in XCGD GT mice were considered spontaneous or related to irradiation, because they also occurred in XCGD UT and Mock mice.

Some XCGD GT mice showed evident signs of disease. One XCGD GT mouse was euthanized 39 weeks after transplantation because of poor health conditions, and based on the microscopic observation, the cause of morbidity could not be determined (Table S2). Diffuse lymphoblastic lymphomas were seen in one XCGD UT (TM035-20) euthanized at 41 weeks after treatment and in one XCGD GT mouse (TM035-29) euthanized at 27 weeks after treatment. T cell origin of lymphomas was

confirmed by CD3 immunostaining of the thymus (Figure 5A). The lymphoma cells in the thymus, spleen, and BM of the mouse TM035-29 had an average VCN of ~ 3.5 , and Gp91^{phox} protein driven by the MSP was undetected (Figure 5B; Table S3).

One XCGD GT mouse (TM035-22) was found dead at 28 weeks after treatment with an enlarged spleen, and lymph nodes showed diffuse myeloid leukemia, as confirmed in the thymus by immunoreactivity for MPO (Figure 6A; Table S2). Analysis of the hematopoietic progenitor compartment revealed an expansion of a population phenotypically resembling GMLP (Lin⁻ sca-1⁺ c-kit⁺ CD48⁺ CD150⁻) and GMP (Lin⁻ c-kit⁺ CD48⁺ CD150⁻) progenitors (Figure 6B). The leukemic cells expressed Gp91^{phox}, and VCN was on average ~ 9 and ~ 7 in the BM and spleen, respectively (Table S3).

We performed a retrospective analysis of all XCGD GT mice used in previous laboratory-grade efficacy studies, and identified 1 out of 14 XCGD GT mice (RD021-54) with increased spleen weight microscopically characterized as myeloid leukemia with massive infiltration of myeloid cells expressing Gp91^{phox} (Figures S5A–S5D). Similar to the TM035-22 mouse, flow cytometry analysis confirmed an

abnormal colored lungs, skin wound, and enlarged liver and spleen correlating with systemic inflammatory conditions, characterized by abscesses with colonies of bacteria, increased diffuse neutrophilic inflammatory cell infiltrate, acidophilic macrophagic pneumonia at microscopic analysis, and thus considered the cause of morbidity. Delayed manifestations of irradiation, as moderate to marked glomerulonephropathy associated with hemorrhages, thrombosis, necrosis, depletion of lymphoid cells in lymphoid tissues, and presence of fluid in the thoracic cavity, were considered the cause of death and morbidity in 4 out of 9 euthanized XCGD Mock mice between 40 and 51 weeks after treatment and in 1 out of 4 XCGD GT mice at 41 weeks post-treatment. Adenocarcinoma with metastasis in mesenteric lymph nodes with abscesses, necrosis, and neutrophilic cell infiltrates in the liver and sarcoma of the skin with systemic inflammation were considered the cause of morbidity in 2 out of 9 XCGD Mock mice at 29 weeks after treatment.

Changes related to pre-transplant conditioning (glomerulonephropathy, lens degeneration, seminiferous tubule degeneration, hypertrophy of the zona fasciculata of adrenal glands, decreased cellularity of lymphocytes in lymphoid organs) were detected in XCGD Mock and

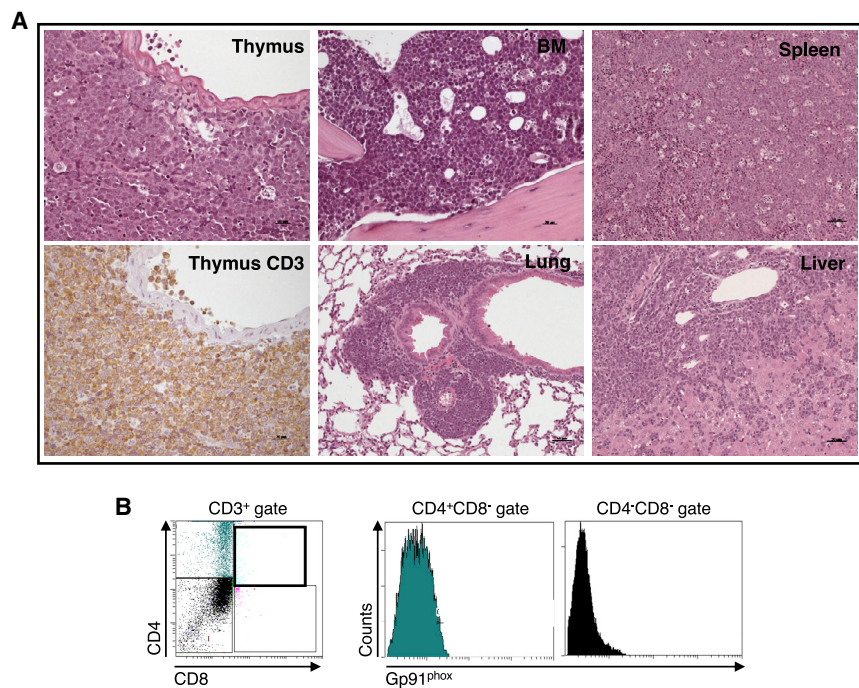


Figure 5. Histopathological and Flow Cytometry Analysis of Organs of XCGD GT Mice with Lymphoblastic Leukemia

(A) H&E staining of representative sections of thymus, BM, spleen, lung, and liver from the XCGD GT mice presenting diffuse lymphoblastic lymphoma (TM035-29) as confirmed by CD3 staining. Original magnification for thymus and BM is 400 \times , scale bars: 50 μ m; original magnification of lung, spleen, and liver is 200 \times , scale bars: 20 μ m. (B) CD4 and CD8 profiles from XCGD and WT mice thymocytes isolated from mouse TM035-29 with lymphoblastic leukemia. Gp91 expression in single-positive CD4 and double-negative CD4 CD8 was also shown.

accumulation of an undifferentiated GMP-like phenotype in the BM (Figure S5C). We noted high VCN in the peripheral blood (37), spleen (39), and BM (29) of the mouse RD021-54.

The overall prevalence rate of lymphoblastic lymphoma was 4.16% (1/24) in the XCGD UT group and 2.94% (1/34) in the XCGD GT group, while myeloid leukemia was 5.88% (2/36) in XCGD mice transplanted with transduced XCGD HSPCs and none in the other groups. Statistical analysis of the tumor incidence was performed using Fisher's exact test for the following comparisons: knockout (KO) GT versus KO Mock, KO GT versus KO UT, KO UT versus KO Mock, and no significant difference was found among the considered pairs of groups.

The XCGD Disease Background May Contribute to Malignant Transformation of Myeloid Cell Precursors upon LV-Mediated GT

The appearance of neoplastic transformation in XCGD GT mice prompted us to investigate whether chronic tissue inflammation typical of the XCGD mouse model could predispose LV-transduced HSPCs to develop myeloid leukemia. We thus transplanted XCGD Lin⁻ cells transduced with the MSP.Gp91.2T vector in lethally irradiated C57BL/6 CD45.1 mice (n = 12) (Table S1). The tumorigenic potential of transduced cells infused in WT mice was assessed for up to 34 weeks and compared with UT CD45.1 C57BL/6 mice (n = 10) and mice receiving untransduced XCGD HSPCs (n = 16).

Pathological findings similar to those characterizing the CGD model (acidophilic macrophagic pneumonia and granulomatous inflammation) were observed in WT mice transplanted with untransduced

XCGD HSPCs, confirming the transfer of the disease by HSCT and, thus, its immune-mediated origin. These findings were not recognized in UT CD45.1 C57BL/6 and WT mice receiving LV-transduced XCGD HSPCs. Other microscopic changes observed in mice of all groups were incidental changes, related to the species background and mouse age. Noteworthy, none of the WT GT mice developed myeloid leukemia, suggesting a possible role of chronic inflammatory XCGD background in promoting transduced myeloid cell progression toward leukemic transformation.

IS Analysis Reveals Reduced Polyclonality in XCGD GT Mice

To assess MSP.Gp91.2T LV genotoxicity, we performed a genome-wide analysis of the LV IS in total BM cells isolated from XCGD GT and WT GT mice at study termination. Overall, a total of 17,520 (average ISs/mouse = 876 \pm 332, range 249–1,457) and 4,439 (average ISs/mouse = 370 \pm 102, range 176–531) ISs were retrieved and mapped from XCGD GT and WT GT mice, respectively (Table S4). The genomic distribution of ISs showed a marked tendency of the MSP.Gp91.2T LV to integrate within gene bodies with no bias for promoter regions, as expected for LV (Figure S6A).

To identify the gene classes preferentially targeted by ISs of the MSP.Gp91.2T vector, we performed an enrichment analysis of annotations associated with the genomic regions targeted by the pooled LV ISs retrieved from XCGD GT and WT GT mice. We found an overrepresentation of gene classes related to nuclear structure, chromatin modification, and other gene classes that have already been described as preferentially targeted by LV insertions as a result of an integration bias of the parental virus rather than genetic selection caused by insertional mutagenesis (Figure S6B).^{10,30,31} Genes recurrently targeted by LV ISs at a frequency higher than expected by a random distribution were recognized by common insertion site (CIS) analysis.³² Overall, five CIS genes were identified in both datasets, none of which, however, was related to cancer (Figure 7A; Table S5). Moreover, we analyzed the gene integration frequency between the two groups (RD027 versus TM035) using a Fisher's exact test adjusted with false discovery rate (FDR), where the two dichotomic variables of the

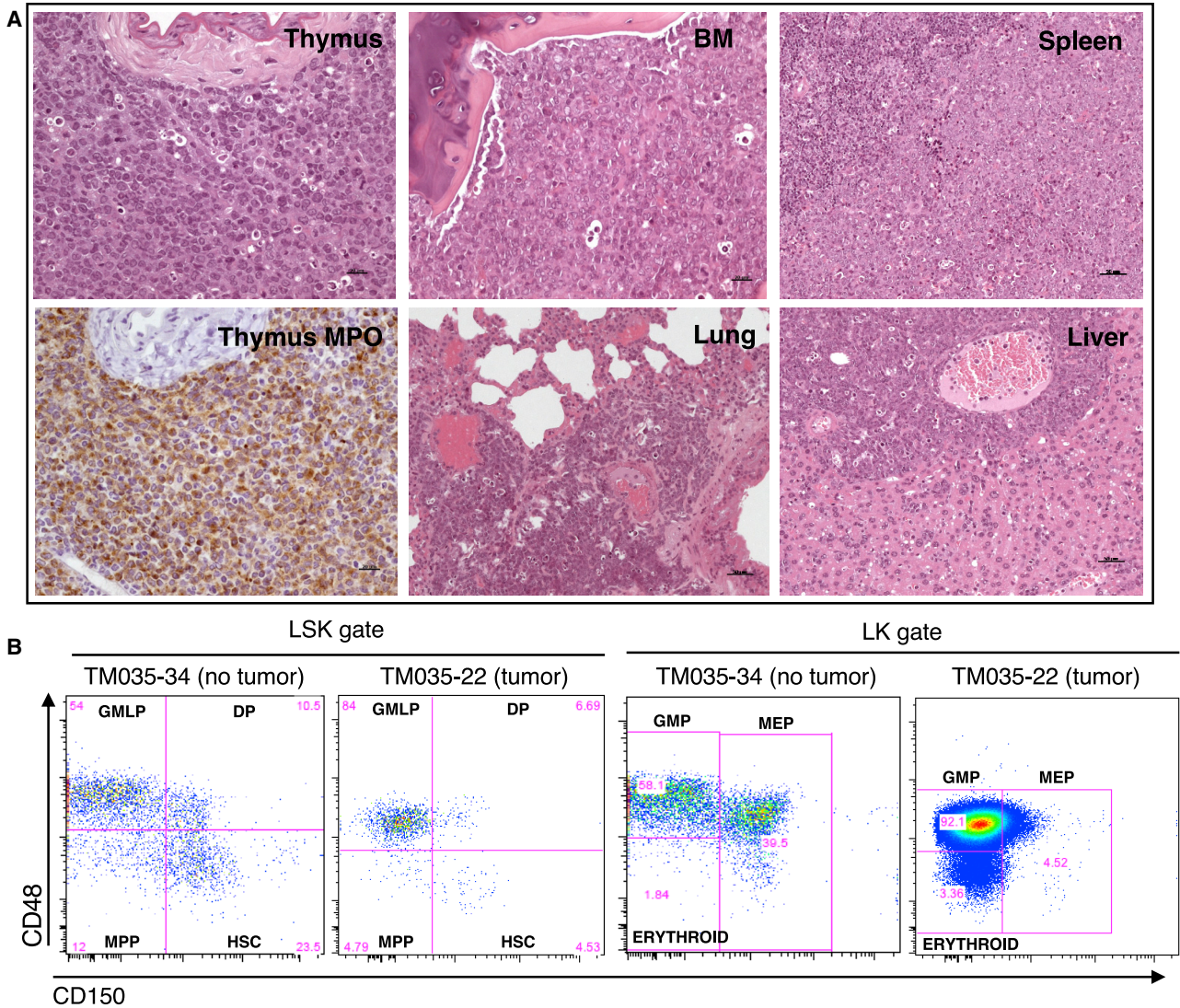


Figure 6. Characterization of Myeloid Leukemia Developed in Some XCGD GT Mice

(A) H&E staining of representative sections of the thymus, BM, spleen, lung, and liver from the XCGD GT mice (TM035-22) with diffuse myeloid leukemia as confirmed by MPO staining. Original magnification for thymus and BM is 400 \times , scale bars: 50 μ m; original magnification of lung, spleen, and liver is 200 \times , scale bars: 20 μ m. (B) Representative immunophenotypic analysis of BM cells isolated from XCGD GT mice with myeloid leukemia. HSC and different progenitors were identified within the Lin⁻ sca-1⁺ c-kit⁺ (LSK) and Lin⁻ c-kit⁺ (LK) gates by the cell surface markers indicated.

contingency matrix are “belonging or not to a gene,” thus reporting the number of ISs targeting that gene on all the other ISs. We selected genes with a number of ISs > 2. None of the 337 genes with ISs higher than 2 resulted in significant targeting ($p < 0.05$), thus demonstrating that the CIS targeting frequency is not statistically different between the two studies (Figure S6C).

To address the clonality of the reconstituted hematopoietic system in XCGD GT and WT GT mice, we analyzed the diversity of the clonal population in each mouse measured by the Shannon diversity index (Figure 7B). BM cells isolated from WT GT and most of the XCGD

GT mice (16/20) showed a polyclonal repertoire with an average Shannon diversity of 4.75 ± 0.29 , except BM cells isolated from XCGD GT mice TM035-22, -29, -39, and -40, which showed reduced clonal diversity (average Shannon diversity index 2.7 ± 0.47). No significant difference was found by comparing the average diversity index between the groups (Wilcoxon test; Figure 7B). Most of the marked cell clones of post-transplantation BM samples had a relative abundance of <10% (Figure 7C). In XCGD GT TM035-22, -29, -39, and -40 mice, we observed few clones with high abundance (>10%), highlighting the oligoclonal IS pattern in these mice, in line with their lower Shannon diversity index (Figure 7B). In the BM samples of

oligoclonal mice, we observed clusters of three to nine ISs with a similar relative abundance and those were dominant compared with the remaining ISs (<10%), suggesting a common clonal origin. Indeed, with the high transduction levels achieved in this study, clones with multiple integrations are expected to be relatively frequent. For instance, BM cells of the XCGD GT TM035-22 mouse developing myeloid leukemia had a cluster of abundant ISs targeting the *Epha7*, *Trib2*, *Sepp1*, *Kctd4*, *Pros1*, and *Rcl1* genes and the oncogene *Ahi1* (Figure 7C). *Sesn1* and *Adgrl2* genes, along with the proto-oncogene *Top1*, were among the most abundant in BM cells of the XCGD GT TM035-29 mouse with lymphoblastic lymphoma. Although the TM035-39 and TM035-40 mice of the XCGD GT group did not develop any apparent neoplastic disease, ISs in the cancer-associated *MDS1-Evi1* and *Etv1* genes were identified among the most abundant clones (Figure 7C). Moreover, the proto-oncogenes *Ahi1*, *Mecom*, *Bcl11a*, and *Etv1* were targeted in additional mice multiple times and ranked among the most abundant ISs (Table S7). The expression of some of the genes targeted in the most abundant clones was assessed in the total BM cells isolated from all of the XCGD GT and WT GT mice. We found significant downregulation of *Mecom* expression in the BM of KO GT mice compared with WT GT mice, whereas the expression of *Etv1*, *Top1*, *Ahi1*, and *Ppp6c* was comparable (Figure S7), suggesting that there is no evidence of transactivation of these genes by the vector integration.

To trace the dynamics and clonal heterogeneity of the leukemic cell population *in vivo*, we adoptively transferred the splenocytes of the XCGD GT mouse RD021-54 with myeloid leukemia into three non-obese diabetic severe combined immunodeficiency (NOD-SCID) IL-2R γ^{null} (NSG) mice. Leukemic cells readily emerged in the peripheral blood of secondary NSG recipients, which were euthanized at 43 days post-transplant because of poor health conditions. Vector-positive cells were detected in peripheral blood leukocytes (VCN = 24.7) and BM (VCN = 25.4) at the study endpoint (Table S6). IS analysis was performed in samples from peripheral blood, spleen, and BM of the mouse RD021-54 and secondary recipients. We identified a total of 738 and 234 unique ISs in the primary RD021-54 mouse and secondary recipient NSG mice, respectively. Clonal tracking analysis revealed a progressive enrichment of clones in the peripheral blood over time and BM at termination, indicative of an ongoing clonal expansion. In contrast, samples from the control mouse RD021-51 with no tumor showed a highly polyclonal vector integration profile (Figure 7D; Figure S8). The identification of the

same number of identical ISs in all secondary NSG mice indicates that the leukemia was monoclonal. ISs in the proximity of some oncogenes, such as *Myb*, *Mpp7*, *Zbtb7a*, and *Cblb*, were identified (Figure 7D). Some of the top ISs found in the PB and BM samples from mouse RD021-54 at euthanasia were also highly present among all samples from secondary recipient NSG mice, indicating the detection of tumor-marking clones.

The observations that WT mice receiving transduced XCGD BM cells showed a sizable polyclonal repertoire of LV integrations and did not develop malignant hematopoietic neoplasia argue against the possibility that vector genotoxicity alone was the cause of myeloid leukemia developing in some XCGD GT mice, and suggest that the inflammatory disease background was also crucial for clonal selection and progression to neoplastic transformation.

DISCUSSION

The present GLP study describes the long-term therapeutic efficacy, toxicity, and tumorigenicity of GT for XCGD based on LV-mediated correction of HSPCs evaluated over 1 year in a large cohort of XCGD mice. The transducing vector used in our experiments was the MSP-Gp91.2T LV recapitulating physiological Gp91^{phox} expression preferentially in myeloid lineage cells.^{26,27} Indeed, sustained Gp91^{phox} expression was detected in myeloid cells, but not T and B cells, of the peripheral blood, spleen, and BM of GT-treated XCGD mice. We also found that LV-driven Gp91^{phox} expression had no adverse effect on the hematopoietic repopulation because transduced HSPCs engrafted and differentiated properly in the peripheral blood, BM, and spleen of XCGD GT-treated mice.

Gp91^{phox} expression in monocytes was stable, but progressively declined in granulocytes over 50 weeks. In contrast, NADPH oxidase activity remained constant in both phagocytes with a significantly higher ROS production in activated granulocytes (58.95 ± 19.70) compared with monocytes (38.65 ± 19.48), suggesting the possibility of an underestimation of the fraction of Gp91^{phox}-expressing cells. Indeed, only the Gp91^{phox} molecules expressed on the cell surface, but not those positioned intracellularly, have been revealed by our staining protocol performed in the absence of permeabilizing agents. It was shown that in resting neutrophils, Gp91^{phox} is found primarily intracellularly in the membrane of secondary granules.^{33,34} Upon activation, these granules are mobilized from these internal compartments to the cell surface or phagosome

Figure 7. Integration Site Analysis of MPS.Gp91.2T LV in Total BM Cells Isolated from XCGD and WT Mice Transplanted with Transduced HSPCs

(A) Volcano plot of CIS analysis results. The gene integration frequency normalized by gene length is represented on the x axis, whereas the y axis shows the p value of CIS Grubbs test for outliers ($-\log$ base 10 of p value). According to the p value, dots are colored in violet if significant (<0.05) and in gray if not. Significant genes are labeled with the gene name, colored according to ontological annotation of tumor suppressor (blue), proto-oncogene (red), and "other" (green). Genes with known clonal expansions have been highlighted with dark red labels (i.e., *Mecom*). (B) Boxplot of clonal heterogeneity measured with the Shannon diversity index. Wilcoxon test on the average entropy between the two groups resulted in not significant. (C) Boxplot representation of clonal abundance in mice. For each sample, IS abundance had been measured as the relative percentage of observed genomes on the total number of genomes in that sample. ISs with abundance above 10% are labeled with the closest gene name (RefSeq mm9). (D) Heatmap representation of the top 50 LV-targeted genes identified in the peripheral blood, BM, and spleen of secondary recipient NSG mice shared with the XCGD GT mouse RD021-54 with myeloid leukemia. Follow-up (FU) are 6, 12, 20, and 33 weeks for the peripheral blood and 33 weeks for the BM of XCGD GT mouse RD021-54, whereas the secondary recipient NSG mice were sacrificed after 43 days.

membrane.³⁵ In steady-state monocytes/macrophages, Gp91^{phox} localizes to both the plasma membrane and the endocytic recycling compartment. Therefore, it appears that the percentage of the Gp91^{phox+} cells may be an underestimate for granulocytes and not for monocytes. Another possibility is a progressive decline in the number of transduced granulocytes due to their short half-life when they reach the bloodstream. Although we did not have direct evidence for transduction levels in granulocytes, the average of the VCN calculated in the total blood leukocytes mirrored the DHR trend. The VCN dropped from 11 to 30 weeks, then remained stable at three to four copies at 50 weeks. The first VCN decline is in line with higher gene transfer into progenitors than stem cells and may explain the diminished Gp91^{phox} staining, but not the DHR assay. The second drop between 30 and 50 weeks may be caused by some degree of vector silencing (even though we do not have direct evidence for this), again amplified by the suboptimal staining procedure for Gp91^{phox}.

Histopathological analysis of a wide range of tissues revealed that gene-corrected granulocytes and monocytes were able to markedly improve most of the hallmark features of mouse XCGD (systemic inflammation, hemorrhages, extramedullary hematopoiesis) and eradicate pulmonary inflammation and bacteria-containing abscesses in GT-treated XCGD mice. Correction of XCGD symptoms markedly improved the morbidity and mortality of XCGD mice, bringing the 1-year survival rate up from 40% to 80%. The long-term phenotypic correction of XCGD pathology in the mouse model highlights the potential therapeutic benefit of the LV-mediated *ex vivo* GT approach for XCGD patients.

Important concerns that our study revealed are the potential toxicity and tumorigenicity associated with MSP.Gp91.2T LV-transduced HSPCs in XCGD mice. Clinical chemistry parameters monitored in the plasma during the study and at termination revealed no biochemical toxicity in the liver, pancreas, kidney, and cardio-circulatory system. However, 4 (20%) XCGD mice died between 27 and 42 weeks. A detailed pathological examination revealed that two mice had died of hematological malignancies, namely, a lymphoblastic lymphoma and myeloid leukemia, occurring at 27 and 28 weeks post-transplant, respectively. The other two XCGD mice presumably died of renal injuries and inflammatory-associated changes in lungs. None of the long-term surviving XCGD GT mice exhibited leukemia-associated symptoms.

From the integrated analysis of the GLP study and additional laboratory-grade experimentations, we observed the development of T cell lymphomas in the XCGD UT (1/24, 4.16%) and GT (1/34, 2.94%) groups. Cells from the thymus, BM, and spleen of the XCGD GT mouse with the lymphoma were vector positive (VCN ~3.5) but did not express Gp91^{phox}, consistent with the fact that the transgene is expressed only in myeloid cells. Lymphomas of the T cell and B cell lineage commonly develop in many strains of mice, including C57BL/6, at an incidence rate of 10%–50% in aging mice.³⁶ Incidence is accelerated and/or enhanced by irradiation, which results in early mortal-

ity.^{37,38} In light of these observations, it seems likely that this type of tumor is associated with irradiation and the disease background, although we cannot exclude a possible contribution of LV-mediated genotoxicity. Two out of 34 mice (5.88%) receiving HSPC GT developed a myeloproliferative syndrome. Peripheral blood and BM of these mice were positive for Gp91^{phox}, indicating that myeloid leukemia originated from transduced donor cells. Statistical analysis revealed no significant difference in tumor incidence rates for KO GT versus KO Mock or KO UT. This was expected because of the sporadic appearance of tumors and the small sample size of mice per group.

Although a large number of different ISs were found in most XCGD GT mice indicative of a sizable polyclonal distribution of LV corrected HSPCs, BM cells of the XCGD GT mice developing myeloid leukemia revealed a low clonal diversity reflected by the high dominance of a few clones. Once transplanted into immunocompromised recipient mice, leukemic clones harboring a similar IS pattern rapidly expanded, indicating that they derive from the original tumor. Most abundant clones harbored LV integrations targeting *Epha7*, *Trib2*, *Kctd4*, *Sepp1*, *Pros1*, and *Myb* genes that have not been reported as oncogenes or tumor suppressor genes associated with insertional mutagenesis for leukemia or lymphoma development. No hotspots of integrations were identified within *Mds1-Evi1*, *Lmo2*, *Prdm16*, and *Setbp1* genes, well-established hallmarks of insertional mutagenesis in mice and clinical trials,^{16,19,39,40} including XCGD. Overall, the IS analysis showed that oligoclonal reconstitution has occurred in some XCGD GT mice. Although IS analysis shows no enrichment of IS targeting oncogenes, some vector insertions near oncogenes, such as *Ahi1*, *Mecom*, *Etv1*, *Myb*, and other cancer-related genes, have been found among the most abundant cell clones in mice with oligoclonal reconstitution. Despite the concerns raised by these observations, no overexpression of the oncogenes targeted by LV ISs in the oligoclonal samples was observed, suggesting that the ISs were neutral.

To the best of our knowledge, this is the first report to describe a possible association between LV-mediated GT and an increased risk for myeloid leukemia in preclinical GT studies for XCGD. A myelodysplastic syndrome secondary to insertional mutagenesis occurred in phase I/II trials for XCGD in patients receiving CD34⁺ cells transduced with an LTR-driven γ -RV.^{16,19,21} Before this work, toxicity studies conducted in mice using a similar LV-mediated approach targeting Gp91^{phox} expression in phagocytes reported no significant adverse events related to GT treatment.^{24,25} Moreover, the lentiviral G1XCGD vector recently used in a multicenter trial did not show any infusion-related adverse events over 24-month follow-up,²⁸ similarly to other diseases treated with HSPC GT.⁴⁰

Some of the differences between the mouse studies can be attributed to the variations in the experimental design.^{24,25} First, in our study, XCGD GT mice were monitored for up to 1 year, whereas the maximum duration of the post-transplant follow-up previously reported was 6 months. Because XCGD GT mice developed myeloid

leukemia starting from 7 months after GT, it is possible that the onset of possible adverse events could have been unnoticed by Brendel et al.²⁵ Second, a contributing factor can be the numerosity of mice analyzed. Earlier tumorigenicity studies have been conducted on far fewer mice per each experimental group ($n = 5-7$), and thus this setting reduced the probability of occurrence of tumors. Third, the different results may have been exacerbated by our higher MOI transduction conditions compared with previous studies, which may have amplified the risk for insertional mutagenesis events. Fourth, the design of MSP.Gp91.2T vector slightly differs from the G1XCGD.²⁵ The MSP promoter used to drive physiological Gp91^{phox} expression in phagocytes was composed of a minimal promoter sequence from the Gp91^{phox} locus fused to the SP146 synthetic enhancer/promoter.^{26,41} It is possible that this design may have increased the oncogenic risk compared with the G1XCGD vector, which comprises a chimeric promoter containing binding sites for PU.1 and C/EBP- α transcription factors expressed by the myeloid lineage.²⁴ Another difference between the two vectors is the incorporation of two miR-126 target sites into the 3' UTR of the Gp91^{phox} expression cassette of MSP.Gp91.2T to allow the degradation of Gp91^{phox} mRNA in HSCs, thereby limiting the ROS-mediated toxicity in these cells.²⁶

One of the most remarkable differences between our and a previous study²⁵ can be attributed to the use of different mouse models. Brendel et al.²⁵ utilized healthy mice, in place of XCGD mice, as sources for both donor Lin⁻ cells and recipient mice. Whenever XCGD mice were used, the longest follow-up period was 4 months. Although WT mice are commonly accepted for *in vivo* toxicology and genotoxicity studies, the mouse model of human disease is of the highest value because it enhances not only the predictability of toxicity of a medicinal product but also allows understanding of the mechanisms of toxicity. This viewpoint is particularly relevant for XCGD, because the use of the disease mouse model, which mimics the clinical situation, allows a more accurate evaluation of potential adverse events, including tumors, during GT experimentations. Indeed, when we examined the effect of disease background on genotoxicity and tumorigenicity related to GT treatment, we made some interesting observations. Transplantation of untransduced XCGD HSPCs caused the appearance of the pathological hallmarks related to the XCGD phenotype, confirming the immune-mediated origin of the disease. We also confirmed in WT recipient mice that, upon GT, most of the XCGD symptoms were markedly reduced. In stark contrast with findings obtained in XCGD recipient mice, none of the WT mice transplanted with transduced XCGD HSPCs developed adverse events, including proliferative lesions. This could be because of the too-small sample size of WT GT mice analyzed. Indeed, assuming a similar rate of tumor incidence in KO GT and WT GT groups, one would not expect to identify mice with leukemias. However, IS analysis revealed a polyclonal distribution in all mice with no abnormal clonal expansion, with exceptions for few clones above 20% for one mouse. CISs revealed no tumor suppressor or oncogenes in the top targeted genes. By comparing the

two studies, we did not observe significant differences in terms of gene frequency and IS abundance.

The high VCN, along with the inflammatory stress hematopoiesis, could have contributed to the observed likelihood of leukemia/lymphoma development. Although not significant, the clear separation of tumor occurrence in KO GT versus WT GT mice receiving the same XCGD cells transduced with the same vector may suggest an implication of the disease background as a potential critical risk factor influencing the fitness of gene-corrected cells, thereby enhancing the potential myeloid transformation of stem-cell-derived clones. Consistently, there is evidence that hyperinflammation in patients and mice with XCGD severely affects the HSC compartment by promoting cell cycling of quiescent HSPC cells.⁴² We observed an expansion of F4/80⁺ histocytes/macrophages and MPO⁺ myeloid cells in the BM and spleen, respectively, of XCGD mice. We also found elevated levels of inflammatory cytokines (IL-1 β , CCL5, and IL-12p40) in the BM milieu collected from XCGD mice compared with age-matched WT control mice. It was shown that blocking *in vivo* IL-1-mediated inflammation by IL-1 receptor antagonist can revert in part the hematopoietic dysfunction in XCGD mice.⁴² It is therefore possible that a hyperinflammatory microenvironment together with radiation-induced damage of the BM niche, as such, cooperates with insertional mutagenesis to favor in the early phase the development of dominant clones harboring LV insertions toward progression into malignancy. Therefore, halting inflammation in patients with XCGD could be relevant for two reasons. On the one hand, the administration of anti-inflammatory, immune modulators before GT procedure could reduce HSC stress and improve both the quality and the quantity of the HSPCs collected. On the other hand, blockade of inflammatory cytokines during GT could restore the physiological self-renewal activity of HSCs, thereby limiting chronic overproduction of myeloid cells, genomic instability, and potentially the acquisition of somatic mutations.

Our study confirms and extends prior reports that LV-mediated *ex vivo* GT for XCGD might be an effective approach to guarantee a long-term correction of the disease. We have also uncovered a potential contribution of the XCGD inflammatory background, along with high VCN, that may have favored the clonal expansion of some transduced HSPCs, eventually leading to the development of leukemia and/or lymphoma. Future preclinical studies with a much larger number of mice would be needed to reveal these sporadic adverse events occurring in the XCGD mouse model and reach some statistical power.

MATERIALS AND METHODS

Mice

B6.129S-Cybb^{m1}Din/J mice (Cybb^{-/-} mice, stock #002365) on a C57BL/6J background were purchased from The Jackson Laboratory, and C57BL/6N CD45.1 and NSG were mice from Charles River. Mice were maintained at IRCCS San Raffaele Scientific Institute SPF Animal Facility under specific pathogen-free conditions. All experimental procedures were approved by the Animal Care and Use Committee of

the Fondazione San Raffaele del Monte Tabor (IACUC 647) and communicated to the Ministry of Health and local authorities in accordance with the Italian legislation.

LV Production

A third-generation self-inactivating vesicular stomatitis virus (VSV.G)-pseudotyped LV was constructed on a pCCL backbone, as previously described.^{43,44} The non-GMP MPS.126T LV lots were produced and purified by MolMed S.p.A. (Milan, Italy).

Transduction and Transplantation of Murine Hematopoietic Progenitors

BM cells were collected by flushing from femurs and tibias of a pool of male and female XCGD mice. Lin⁻ HSPCs isolated using the Lineage Cell Depletion Kit (Miltenyi) were cultured in Stem Span serum-free expansion medium (Stem Cell Technologies) supplemented with 1% L-glutamine, 1% penicillin/streptomycin, murine stem cell factor (SCF; 100 ng/mL), murine thrombopoietin (TPO; 50 ng/mL), human Flt3L (100 ng/mL), and human IL-3 (20 ng/mL; all from PeproTech) for 2 h. Cells were then cultured in the presence or absence (Mock) of a clinical preparation of MSP.Gp91.2T LV at an MOI of 200 for 16 ± 2 h.

Untransduced and transduced cells (1 × 10⁶/mouse) were injected intravenously in lethally (9 Gy split into two equal doses) irradiated 7- to 9-week-old XCGD male mice (XCGD GT mice, n = 20). Only male mice have been used in consideration of the fact that X-linked CGD usually affects only males. Mice were monitored for 52 weeks. Lin⁻ HSPCs isolated from XCGD mice and transduced or not with the MSP.Gp91.2T LV (0.5 × 10⁶/mouse) were injected intravenously in lethally (9 Gy split into two equal doses) irradiated 7- to 9-week-old WT CD45.1 male and female mice (XCGD GT WT mice, n = 12), and mice were monitored for 34 weeks.

Secondary Transplant of Myeloid Leukemia

Splenocytes of the XCGD GT mouse RD021-54 (1.5 × 10⁶/mouse) were injected intravenously into irradiated (1 Gy) 7- to 8-week-old NSG female mice (n = 3) and monitored daily for 43 days.

Measurements of Transduction Efficiency

After transduction, cells were cultured in liquid culture medium (Stem Span medium supplemented with 10% v/v fetal bovine serum [FBS], 1% L-glutamine, 1% penicillin/streptomycin [P/S], mSCF [100 ng/mL], mTPO [50 ng/mL], hFlt3L [100 ng/mL], and hIL-3 [20 ng/mL]; all from PeproTech) for 3 days. To promote myeloid differentiation, medium was removed, and cells were maintained in cell expansion myeloid differentiation medium (RPMI supplemented with 10% v/v FBS, P/S, 1% L-glutamine, and mouse G-CSF [100 ng/mL]) for an additional 14 days. Transduction efficiency was evaluated by qPCR using a primers/probe set designed in the common packaging signal region (Psi) of LVs upstream of the gag start codon, as previously described.⁴⁵ Mouse *β-actin* was used as the housekeeping gene (the list of primers and probes sequences is shown in Table S8). VCN was determined on genomic DNA extracted from

transduced cells after *in vitro* culture for 14 days and single hematopoietic CFUs. Colonies were defined as negative CFUs when the VCN was <0.5 copy/genome and as positive when >0.5 copies/genome. Transduction efficiency was calculated as number of positive CFUs × 100/number of total CFUs.

Blood Chemistry Tests

Peripheral blood samples were collected from the tail vein in the absence of anti-coagulant at 15 and 52 weeks post-treatment. The serum was separated at room temperature by centrifugation. Analyses were performed by the Research Toxicology Centre S.p.A (Pomezia, Rome, Italy).

Hemocytometer Analysis

Red blood cells (RBCs), HGB, PLTs, and total WBCs were measured in the peripheral blood of mice using the Procyte DX Analyzer (IDEXX) at 11, 30, and 50 weeks upon treatments.

Flow Cytometry Staining

Blood (~50 μL) was withdrawn from the tail vein in EDTA-coated tubes at 11, 30, and 50 weeks post-treatment. Blood was incubated with RBC lysis buffer to remove erythrocytes (ACK buffer for 10 min at room temperature [RT]). BM cells were harvested at 52 weeks. Cells were incubated with (Fc) blocking and labeled with the following antibodies for 30 min at 4°C: anti-CD3, anti-CD48, anti-B220 (CD45RA), anti-CD11b, anti-Ly6G, and anti-Gp91^{phox}. Cells were acquired on a Gallios flow cytometer (Beckman Coulter). Percentages of lymphoid (CD3⁺ T cells, B220⁺ B cells) and myeloid cells (CD11b⁺ Ly6G⁺ granulocytes, CD11b⁺ CD48⁺ monocytes) were determined within the CD45.2⁺ cells, and then the proportion of cells expressing the human Gp91^{phox} was calculated for each subpopulation.

The frequency of stem and progenitor cells was evaluated in total BM preparations isolated from age-matched XCGD UT, Mock, and GT mice at study termination (50 ± 2 weeks) by flow cytometry. Cells (6 × 10⁶) were labeled with the following antibodies: lineage cocktail (CD3, Ly-6G/Ly-6C, CD11b, CD45R/B220, and TER-119), CD45.2, sca-1/Ly-6A/E, c-kit/CD117, CD48, and CD150. The list of the antibody clones and fluorochromes is included in Table S9. Samples have been acquired using a BD FACSCanto II system and analyzed with the BD FACSDiva Software. On the CD45.2 gate, the long-term repopulating HSCs were identified as Lin⁻ sca-1⁺ c-kit⁺ CD48⁻ CD150⁺, MPP as Lin⁻ sca-1⁺ c-kit⁺ CD48⁻ CD150⁻, GMLP as Lin⁻ sca-1⁺ c-kit⁺ CD48⁺ CD150⁻, GMP as Lin⁻ sca-1⁻ c-kit⁺ CD48⁺ CD150⁻, erythroid progenitors (ERY) as Lin⁻ sca-1⁻ c-kit⁺ CD48⁻ CD150⁻, and megakaryocyte-erythroid progenitors (MEPs) as Lin⁻ sca-1⁻ c-kit⁺ CD48⁺ CD150⁺ cells.

Engraftment of Transduced Cells

The average VCN per cell was determined by qPCR using the instrument ViiA 7 Real-Time PCR System (Applied Biosystems). Blood, spleen, and BM DNA were purified using the QIAmp DNA Blood

Mini Kit (Qiagen) and amplified by qPCR (Table S8), as already described.⁴⁵

NADPH Oxidase Activity

Blood (~100 μ L) was withdrawn from the tail vein in heparin-coated tubes at 11, 30, and 50 weeks post-treatment, and BM cells were incubated with RBC lysis buffer to remove erythrocytes (ACK buffer for 10 min at RT). NADPH oxidase activity was determined by flow cytometry as rhodamine 123 generation derived from ONOO⁻-dependent oxidation of DHR123.²⁹ In brief, cells were incubated at 37°C for 10 min with allophycocyanin (APC)-conjugated anti-mouse CD11b, Pacific Blue-conjugated CD48, and phycoerythrin (PE)-conjugated Ly6G antibodies in PBS-gg (PBS with 0.1% gelatin and 0.09% D-glucose) containing catalase (1,000 U/mL) and DHR123 (2 μ g/sample; Sigma-Aldrich). To activate NADPH oxidase, we incubated cells with phorbol myristate acetate (PMA; 500 ng) at 37°C. After 15 min, the reaction was stopped on ice, and cells were analyzed immediately on a FACSCanto II (BD Biosciences). DHR123⁺ cells were gated on CD11b⁺ CD48⁺ monocytes and CD11b⁺ Ly6G⁺ granulocytes.

Cytokine Measurement

Cytokines were measured in the BM fluid collected from UT XCGD and WT mice using the Bioplex Mouse Cytokine Standard Plex (Bio-Rad), according to the manufacturer's instructions.

Histopathological Analysis

A full necropsy was performed, and gross observations were recorded in all mice. The following organs were collected: adrenal glands, BM (right femur and tibia, sternum), brain, cecum, colon, duodenum, eyes with optic nerves, heart, ileum, jejunum, kidneys, liver together with gall bladder, lungs, lymph nodes (mandibular and mesenteric), rectum, salivary glands, spleen, stomach, testes, thymus, and macroscopic abnormalities. Organs were fixed in 10% buffered formalin, trimmed and embedded in paraffin wax, sectioned, and stained with hematoxylin and eosin for histological examination. Selected slides were stained with monoclonal rat anti-human CD3 (Bio-Rad), rat anti-mouse B220/CD45R (clone RA3-6B2; Bio-Rad), and rat anti-mouse F4/80 (clone CI: A31; Bio-Rad) after antigen retrieval. Immunoreactions were revealed using a rat on rodent HRP-polymer (Biocare Medical) and the 3,3 diaminobenzidine (DAB) as chromogen (Biocare Medical). Slides were then counterstained with hematoxylin. Histopathological examination was performed by board-certified pathologists on all tissues of the study animals. A peer review was performed by a second board-certified pathologist on all mice with significant histological findings, including all neoplasia, according to GLP SR-TIGET Test Facility Standard Operating Procedures.

IS Analysis

For the retrieval of vector ISs from TM035 and RD027 groups of mice, we adopted a sonication-based linker-mediated (LM) PCR method on genomic DNA isolated from total BM cells, as described previously.^{46,47} In brief, genomic DNA (300 ng) was sheared using a Covaris E220 Ultrasonicator (Covaris, Woburn, MA, USA), generating

fragments with a target size of 1,000 bp. The fragmented DNA was split into three parts to generate technical replicates and, by using the NEBNext Ultra DNA Library Prep Kit for Illumina (New England Biolabs, Ipswich, MA, USA), subjected to end repair, 3' adenylation, and ligation to linker cassettes (Integrated DNA Technologies, Skokie, IL, USA) containing a 8-nucleotide sequence barcode used for sample identification, a 12-random-nucleotide sequence used for quantification purposes, and all the sequences required for the Read 2 Illumina paired-end sequencing, tracked within our laboratory information management system.^{48,49} Ligation products were then subjected to 35 cycles of exponential PCR using primers specific for the LV LTR and the linker cassette. The amplification product is then re-amplified with an additional 10 PCR cycles using a primer specific for the linker cassette and the LTR (containing ID barcode and random sequences and compatible for Read 1 Illumina sequencing) and sequenced using the Illumina HiSeq platform (Illumina, San Diego, CA, USA).

ISs from the RD021 group of mice were retrieved through linear amplification-mediated (LAM) PCR as previously described.⁵⁰

Sequencing reads were processed by a dedicated bioinformatics pipeline (VISPA2) as previously described.⁴⁹ In brief, paired sequence reads are filtered for quality standards, barcodes identified for sample demultiplexing of the sequence reads, the cellular genomic sequence mapped on the human genome (version hg19), and the nearest RefSeq gene assigned to each unambiguously mapped IS. Clonal abundance from (LM)-PCR-processed samples was estimated as described previously,^{46,47} where the number of genomes with the same IS is calculated by counting the number of fragments with different sizes (generated by sonication) belonging to each individual IS and the different random barcodes (12 random nucleotides) attached to each fragment.⁵¹ The relative abundance of each clone is then calculated as the percentage of genomes with a specific IS over the total genomes. CISs were identified by using the Grubbs test for outliers.³² Enrichment analysis for ontological classes among the targeted genes by vector integrations was performed by the Genomic Regions Enrichment of Annotations Tool (GREAT).⁵² Statistical analyses involving ISs have been performed with R software.

For the generation of the heatmap graphs for IS clonal tracking in RD021 mice, we plot sequencing read values through R package gplots (<https://cran.r-project.org/web/packages/gplots/gplots.pdf>) with a scale of color intensities reflecting the amount of sequencing reads for each IS.

Statistical Methods

The pairwise comparison of survival curves in Figure 1A was performed with the log rank test, and p values were adjusted with Bonferroni's correction to account for multiple comparisons. For comparing the distribution of a numerical variable among independent groups, the Mann-Whitney test was employed in case of two groups (Figures 4C; Figure S6), while in case of more than two groups (Figures 1B, 2C, 2D, and 3B; Figures S3B–S3E) the Kruskal-Wallis test

was used, followed by a post hoc analysis performed with Dunn's test when the p value of the test was below the significance level. In Figure 2A, the comparisons of numerical variables among matched groups were performed with Friedman's test, followed by a post hoc analysis performed with the Conover's test when the p value of the test was below the significance level. In the case of longitudinal analysis with a different number of samples at the different time points (Figures 2B and 3A; Figures S2A, S2B, and S3A), comparisons among groups were performed with linear mixed-effect (LME) models. In order to meet the assumption of normality of the residuals of the model, when necessary, an appropriate transformation was applied to the response variable, and eventually, few outliers were not included in the analysis. In particular, the following transformations were applied for the analysis: the percentage of Gp91^{phox+} monocytes and granulocytes (Figure 2B) were transformed with the square and fourth root, respectively; the percentages of DHR⁺ monocytes and granulocytes (Figure 3A) were transformed with the square and cubic root, respectively; total serum protein value (Figure S2A) was raised to the power of four, whereas alanine and aspartate aminotransferase levels were log transformed; RBC, HGB, and PLT counts (Figure S2B) were raised to the power of six, four, and two, respectively; the percentages of T cells, B cells, and monocytes (Figure S3A) were squared, whereas the percentage of granulocytes was log transformed. For testing differences between all pairs of groups at fixed time point or differences among time points for a fixed group, a post hoc analysis was performed by using the R package *phia*. In all types of post hoc analysis, p values were adjusted with Bonferroni's correction to account for multiple comparisons and/or testing. The Fisher's exact test was used for comparing tumor incidence between two groups. p values less than 0.05 were considered significant. All statistical analyses were performed using R 3.5.0 (<http://www.R-project.org>).

SUPPLEMENTAL INFORMATION

Supplemental Information can be found online at <https://doi.org/10.1016/j.ymthe.2020.09.030>.

AUTHOR CONTRIBUTIONS

Study concept, design, and supervision: R.J.H., F.S., P.C., L.N., B.G., E.M., A.A., and A.M. Acquisition of data: R.J.H., A.C., F.D.M., G.F., S.S., I.V., N.C., M.D.S., M.V., F.C., M.M., L.B.-R., M.O., and F.B. Analysis and interpretation of data: R.J.H., A.C., F.D.M., G.F., S.S., M.M., L.B.-R., M.O., F.B., E.M., and A.M. Pathology evaluation: F.S., R.N., and P.C. Statistical Analysis: P.M.V.R. and C.D.S. GLP compliance quality assurance: P.A. Writing of the manuscript: A.M. Writing of sections of the manuscript: R.J.H., A.C., and F.S. Critical revision of the manuscript: F.S., S.S., L.N., B.G., E.M., and A.A.

CONFLICTS OF INTEREST

The authors declare no competing interests.

ACKNOWLEDGMENTS

This work was funded by grants from the European Commission, European Union (E-rare project EURO-CGD and CELL-PID

HEALTH-F5-2010-261387), Fondazione Telethon, Italy (SR-TIGET Core Grant, Project A6), and Italian Ministry of Health (Bando Progetti di Rete, NET-2011-02350069). All authors wish to thank Claudio Doglioni for consultation on pathology analysis; Elisabetta Zino, Luca Monti, and Edoardo Stradella for GLP compliance quality assurance; Michela Gabaldo for the management of the SR-TIGET Alliance with GlaxoSmithKline; and the staff of the Flow cytometry Resource, Advanced Cytometry Technical Applications Laboratory (FRACTAL) for assistance with flow cytometry.

REFERENCES

- Rider, N.L., Jameson, M.B., and Creech, C.B. (2018). Chronic Granulomatous Disease: Epidemiology, Pathophysiology, and Genetic Basis of Disease. *J. Pediatric Infect. Dis. Soc.* 7 (Suppl 1), S2–S5.
- Mahdavian, S.A., Mohajerani, S.A., Rezaei, N., Casanova, J.L., Mansouri, S.D., and Velayati, A.A. (2013). Pulmonary manifestations of chronic granulomatous disease. *Expert Rev. Clin. Immunol.* 9, 153–160.
- Marciano, B.E., Spalding, C., Fitzgerald, A., Mann, D., Brown, T., Osgood, S., Yockey, L., Darnell, D.N., Barnhart, L., Daub, J., et al. (2015). Common severe infections in chronic granulomatous disease. *Clin. Infect. Dis.* 60, 1176–1183.
- Güngör, T., Teira, P., Slatter, M., Stussi, G., Stepensky, P., Moshous, D., Vermont, C., Ahmad, I., Shaw, P.J., Telles da Cunha, J.M., et al.; Inborn Errors Working Party of the European Society for Blood and Marrow Transplantation (2014). Reduced-intensity conditioning and HLA-matched haemopoietic stem-cell transplantation in patients with chronic granulomatous disease: a prospective multicentre study. *Lancet* 383, 436–448.
- Lum, S.H., Flood, T., Hambleton, S., McNaughton, P., Watson, H., Abinun, M., Owens, S., Cigrovski, N., Cant, A., Gennery, A.R., and Slatter, M. (2019). Two decades of excellent transplant survival for chronic granulomatous disease: a supragional immunology transplant center report. *Blood* 133, 2546–2549.
- Morillo-Gutierrez, B., Beier, R., Rao, K., Burroughs, L., Schulz, A., Ewins, A.M., Gibson, B., Sedlacek, P., Krol, L., Strahm, B., et al. (2016). Treosulfan-based conditioning for allogeneic HSCT in children with chronic granulomatous disease: a multi-center experience. *Blood* 128, 440–448.
- Aiuti, A., Cattaneo, F., Galimberti, S., Benninghoff, U., Cassani, B., Callegaro, L., Scaramuzza, S., Andolfi, G., Mirolo, M., Brigida, I., et al. (2009). Gene therapy for immunodeficiency due to adenosine deaminase deficiency. *N. Engl. J. Med.* 360, 447–458.
- Cicalese, M.P., Ferrua, F., Castagnaro, L., Pajno, R., Barzaghi, F., Giannelli, S., Dionisio, F., Brigida, I., Bonopane, M., Casiraghi, M., et al. (2016). Update on the safety and efficacy of retroviral gene therapy for immunodeficiency due to adenosine deaminase deficiency. *Blood* 128, 45–54.
- Shaw, K.L., Garabedian, E., Mishra, S., Barman, P., Davila, A., Carbonaro, D., Shupien, S., Selvin, C., Geiger, S., Nowicki, B., et al. (2017). Clinical efficacy of gene-modified stem cells in adenosine deaminase-deficient immunodeficiency. *J. Clin. Invest.* 127, 1689–1699.
- Aiuti, A., Biasco, L., Scaramuzza, S., Ferrua, F., Cicalese, M.P., Baricordi, C., Dionisio, F., Calabria, A., Giannelli, S., Castiello, M.C., et al. (2013). Lentiviral hematopoietic stem cell gene therapy in patients with Wiskott-Aldrich syndrome. *Science* 341, 1233151.
- Hacein-Bey Abina, S., Gaspar, H.B., Blondeau, J., Caccavelli, L., Charrier, S., Buckland, K., Picard, C., Six, E., Himoudi, N., Gilmour, K., et al. (2015). Outcomes following gene therapy in patients with severe Wiskott-Aldrich syndrome. *JAMA* 313, 1550–1563.
- Ferrua, F., Cicalese, M.P., Galimberti, S., Giannelli, S., Dionisio, F., Barzaghi, F., Migliavacca, M., Bernardo, M.E., Calbi, V., Assanelli, A.A., et al. (2019). Lentiviral haemopoietic stem/progenitor cell gene therapy for treatment of Wiskott-Aldrich syndrome: interim results of a non-randomised, open-label, phase 1/2 clinical study. *Lancet Haematol.* 6, e239–e253.
- Mamcarz, E., Zhou, S., Lockey, T., Abdelsamed, H., Cross, S.J., Kang, G., Ma, Z., Condori, J., Dowdy, J., Triplett, B., et al. (2019). Lentiviral Gene Therapy

- Combined with Low-Dose Busulfan in Infants with SCID-X1. *N. Engl. J. Med.* 380, 1525–1534.
14. Malech, H.L., Maples, P.B., Whiting-Theobald, N., Linton, G.F., Sekhsaria, S., Vowells, S.J., Li, F., Miller, J.A., DeCarlo, E., Holland, S.M., et al. (1997). Prolonged production of NADPH oxidase-corrected granulocytes after gene therapy of chronic granulomatous disease. *Proc. Natl. Acad. Sci. USA* 94, 12133–12138.
 15. Goebel, W.S., and Dinauer, M.C. (2003). Gene therapy for chronic granulomatous disease. *Acta Haematol.* 110, 86–92.
 16. Ott, M.G., Schmidt, M., Schwarzwaelder, K., Stein, S., Siler, U., Koehl, U., Glimm, H., Kühlcke, K., Schilz, A., Kunkel, H., et al. (2006). Correction of X-linked chronic granulomatous disease by gene therapy, augmented by insertional activation of MDS1-EV11, PRDM16 or SETBP1. *Nat. Med.* 12, 401–409.
 17. Bianchi, M., Hakkim, A., Brinkmann, V., Siler, U., Seger, R.A., Zychlinsky, A., and Reichenbach, J. (2009). Restoration of NET formation by gene therapy in CGD controls aspergillosis. *Blood* 114, 2619–2622.
 18. Kang, E.M., Choi, U., Theobald, N., Linton, G., Long Priel, D.A., Kuhns, D., and Malech, H.L. (2010). Retrovirus gene therapy for X-linked chronic granulomatous disease can achieve stable long-term correction of oxidase activity in peripheral blood neutrophils. *Blood* 115, 783–791.
 19. Stein, S., Ott, M.G., Schultze-Strasser, S., Jauch, A., Burwinkel, B., Kinner, A., Schmidt, M., Krämer, A., Schwäble, J., Glimm, H., et al. (2010). Genomic instability and myelodysplasia with monosomy 7 consequent to EV11 activation after gene therapy for chronic granulomatous disease. *Nat. Med.* 16, 198–204.
 20. Kang, H.J., Bartholomae, C.C., Paruzynski, A., Arens, A., Kim, S., Yu, S.S., Hong, Y., Joo, C.W., Yoon, N.K., Rhim, J.W., et al. (2011). Retroviral gene therapy for X-linked chronic granulomatous disease: results from phase I/II trial. *Mol. Ther.* 19, 2092–2101.
 21. Siler, U., Paruzynski, A., Holtgreve-Grez, H., Kuzmenko, E., Koehl, U., Renner, E.D., Alhan, C., de Loosdrecht, A.A., Schwäble, J., Pfluger, T., et al. (2015). Successful Combination of Sequential Gene Therapy and Rescue Allo-HSCT in Two Children with X-CGD - Importance of Timing. *Curr. Gene Ther.* 15, 416–427.
 22. Montini, E., Cesana, D., Schmidt, M., Sanvito, F., Ponzoni, M., Bartholomae, C., Sergi, L., Benedicenti, F., Ambrosi, A., Di Serio, C., et al. (2006). Hematopoietic stem cell gene transfer in a tumor-prone mouse model uncovers low genotoxicity of lentiviral vector integration. *Nat. Biotechnol.* 24, 687–696.
 23. Modlich, U., Navarro, S., Zychlinski, D., Maetzig, T., Knoess, S., Brugman, M.H., Schambach, A., Charrier, S., Galy, A., Thrasher, A.J., et al. (2009). Insertional transformation of hematopoietic cells by self-inactivating lentiviral and gammaretroviral vectors. *Mol. Ther.* 17, 1919–1928.
 24. Santilli, G., Almarza, E., Brendel, C., Choi, U., Beilin, C., Blundell, M.P., Haria, S., Parsley, K.L., Kinnon, C., Malech, H.L., et al. (2011). Biochemical correction of X-CGD by a novel chimeric promoter regulating high levels of transgene expression in myeloid cells. *Mol. Ther.* 19, 122–132.
 25. Brendel, C., Rothe, M., Santilli, G., Charrier, S., Stein, S., Kunkel, H., Abriss, D., Müller-Kuller, U., Gaspar, B., Modlich, U., et al. (2018). Non-Clinical Efficacy and Safety Studies on G1XCGD, a Lentiviral Vector for Ex Vivo Gene Therapy of X-Linked Chronic Granulomatous Disease. *Hum. Gene Ther. Clin. Dev.* 29, 69–79.
 26. Chiriaco, M., Farinelli, G., Capo, V., Zonari, E., Scaramuzza, S., Di Matteo, G., Sergi, L.S., Migliavacca, M., Hernandez, R.J., Bombelli, F., et al. (2014). Dual-regulated lentiviral vector for gene therapy of X-linked chronic granulomatosis. *Mol. Ther.* 22, 1472–1483.
 27. Farinelli, G., Jofra Hernandez, R., Rossi, A., Ranucci, S., Sanvito, F., Migliavacca, M., Brombin, C., Pramov, A., Di Serio, C., Bovolenta, C., et al. (2016). Lentiviral Vector Gene Therapy Protects XCGD Mice From Acute Staphylococcus aureus Pneumonia and Inflammatory Response. *Mol. Ther.* 24, 1873–1880.
 28. Kohn, D.B., Booth, C., Kang, E.M., Pai, S.Y., Shaw, K.L., Santilli, G., Armant, M., Buckland, K.F., Choi, U., De Ravin, S.S., et al.; Net4CGD consortium (2020). Lentiviral gene therapy for X-linked chronic granulomatous disease. *Nat. Med.* 26, 200–206.
 29. Kooy, N.W., Royall, J.A., Ischiropoulos, H., and Beckman, J.S. (1994). Peroxynitrite-mediated oxidation of dihydrorhodamine 123. *Free Radic. Biol. Med.* 16, 149–156.
 30. Barr, S.D., Ciuffi, A., Leipzig, J., Shinn, P., Ecker, J.R., and Bushman, F.D. (2006). HIV integration site selection: targeting in macrophages and the effects of different routes of viral entry. *Mol. Ther.* 14, 218–225.
 31. Biffi, A., Montini, E., Lorioli, L., Cesani, M., Fumagalli, F., Plati, T., Baldoli, C., Martino, S., Calabria, A., Canale, S., et al. (2013). Lentiviral hematopoietic stem cell gene therapy benefits metachromatic leukodystrophy. *Science* 341, 1233158.
 32. Biffi, A., Bartolomae, C.C., Cesana, D., Cartier, N., Aubourg, P., Ranzani, M., Cesani, M., Benedicenti, F., Plati, T., Rubagotti, E., et al. (2011). Lentiviral vector common integration sites in preclinical models and a clinical trial reflect a benign integration bias and not oncogenic selection. *Blood* 117, 5332–5339.
 33. Borregaard, N., Heiple, J.M., Simons, E.R., and Clark, R.A. (1983). Subcellular localization of the b-cytochrome component of the human neutrophil microbicidal oxidase: translocation during activation. *J. Cell Biol.* 97, 52–61.
 34. Jesaitis, A.J., Buescher, E.S., Harrison, D., Quinn, M.T., Parkos, C.A., Livesey, S., and Linner, J. (1990). Ultrastructural localization of cytochrome b in the membranes of resting and phagocytosing human granulocytes. *J. Clin. Invest.* 85, 821–835.
 35. Borregaard, N., and Cowland, J.B. (1997). Granules of the human neutrophilic polymorphonuclear leukocyte. *Blood* 89, 3503–3521.
 36. Ward, J.M. (2006). Lymphomas and leukemias in mice. *Exp. Toxicol. Pathol.* 57, 377–381.
 37. Vesselinovitch, S.D., Simmons, E.L., Mihailovich, N., Rao, K.V., and Lombard, L.S. (1971). The effect of age, fractionation, and dose on radiation carcinogenesis in various tissues of mice. *Cancer Res.* 31, 2133–2142.
 38. Boorman, G.A., Rafferty, C.N., Ward, J.M., and Sills, R.C. (2000). Leukemia and lymphoma incidence in rodents exposed to low-frequency magnetic fields. *Radiat. Res.* 153, 627–636.
 39. Du, Y., Jenkins, N.A., and Copeland, N.G. (2005). Insertional mutagenesis identifies genes that promote the immortalization of primary bone marrow progenitor cells. *Blood* 106, 3932–3939.
 40. Cavazzana, M., Bushman, F.D., Miccio, A., André-Schmutz, I., and Six, E. (2019). Gene therapy targeting haematopoietic stem cells for inherited diseases: progress and challenges. *Nat. Rev. Drug Discov.* 18, 447–462.
 41. Barde, I., Laurenti, E., Verp, S., Wiznerowicz, M., Offner, S., Viornery, A., Galy, A., Trumpp, A., and Trono, D. (2011). Lineage- and stage-restricted lentiviral vectors for the gene therapy of chronic granulomatous disease. *Gene Ther.* 18, 1087–1097.
 42. Weisser, M., Demel, U.M., Stein, S., Chen-Wichmann, L., Touzot, F., Santilli, G., Sujer, S., Brendel, C., Siler, U., Cavazzana, M., et al. (2016). Hyperinflammation in patients with chronic granulomatous disease leads to impairment of hematopoietic stem cell functions. *J. Allergy Clin. Immunol.* 138, 219–228.e9.
 43. Zufferey, R., Dull, T., Mandel, R.J., Bukovsky, A., Quiroz, D., Naldini, L., and Trono, D. (1998). Self-inactivating lentivirus vector for safe and efficient in vivo gene delivery. *J. Virol.* 72, 9873–9880.
 44. Follenzi, A., Ailles, L.E., Bakovic, S., Geuna, M., and Naldini, L. (2000). Gene transfer by lentiviral vectors is limited by nuclear translocation and rescued by HIV-1 pol sequences. *Nat. Genet.* 25, 217–222.
 45. Capotondo, A., Cesani, M., Pepe, S., Fasano, S., Gregori, S., Tononi, L., Venneri, M.A., Brambilla, R., Quattrini, A., Ballabio, A., et al. (2007). Safety of arylsulfatase A over-expression for gene therapy of metachromatic leukodystrophy. *Hum. Gene Ther.* 18, 821–836.
 46. Firouzi, S., López, Y., Suzuki, Y., Nakai, K., Sugano, S., Yamochi, T., and Watanabe, T. (2014). Development and validation of a new high-throughput method to investigate the clonality of HTLV-1-infected cells based on provirus integration sites. *Genome Med.* 6, 46.
 47. Gillet, N.A., Malani, N., Melamed, A., Gormley, N., Carter, R., Bentley, D., Berry, C., Bushman, F.D., Taylor, G.P., and Bangham, C.R. (2011). The host genomic environment of the provirus determines the abundance of HTLV-1-infected T-cell clones. *Blood* 117, 3113–3122.
 48. Sessa, M., Lorioli, L., Fumagalli, F., Acquati, S., Redaelli, D., Baldoli, C., Canale, S., Lopez, I.D., Morena, F., Calabria, A., et al. (2016). Lentiviral haemopoietic stem-cell gene therapy in early-onset metachromatic leukodystrophy: an ad-hoc analysis of a non-randomised, open-label, phase 1/2 trial. *Lancet* 388, 476–487.

49. Spinozzi, G., Calabria, A., Brasca, S., Beretta, S., Merelli, I., Milanesi, L., and Montini, E. (2017). VISPA2: a scalable pipeline for high-throughput identification and annotation of vector integration sites. *BMC Bioinformatics* 18, 520.
50. Schmidt, M., Schwarzwaelder, K., Bartholomae, C., Zaoui, K., Ball, C., Pilz, I., Braun, S., Glimm, H., and von Kalle, C. (2007). High-resolution insertion-site analysis by linear amplification-mediated PCR (LAM-PCR). *Nat. Methods* 4, 1051–1057.
51. Berry, C.C., Gillet, N.A., Melamed, A., Gormley, N., Bangham, C.R., and Bushman, F.D. (2012). Estimating abundances of retroviral insertion sites from DNA fragment length data. *Bioinformatics* 28, 755–762.
52. McLean, C.Y., Bristol, D., Hiller, M., Clarke, S.L., Schaar, B.T., Lowe, C.B., Wenger, A.M., and Bejerano, G. (2010). GREAT improves functional interpretation of cis-regulatory regions. *Nat. Biotechnol.* 28, 495–501.